Climate Dynamics (1996) 12:557–572

Climate Dynamics

Design and performance of a new cloud microphysics scheme developed for the ECHAM general circulation model

U. Lohmann, E. Roeckner

Max Planck Institute for Meteorology, Hamburg, Germany

Received: 29 November 1995 / Accepted: 4 March 1996

Abstract. A new cloud microphysics scheme including a prognostic treatment of cloud ice (PCI) is developed to yield a more physically based representation of the components of the atmospheric moisture budget in the general circulation model ECHAM. The new approach considers cloud water and cloud ice as separate prognostic variables. The precipitation formation scheme for warm clouds distinguishes between maritime and continental clouds by considering the cloud droplet number concentration, in addition to the liquid water content. Based on several observational data sets, the cloud droplet number concentration is derived from the sulfate aerosol mass concentration as given from the sulfur cycle simulated by ECHAM. Results obtained with the new scheme are compared to satellite observations and in situ measurements of cloud physical and radiative properties. In general, the standard model ECHAM4 and also PCI capture the overall features, and the simulated results usually lie within the range of observed uncertainty. As compared to ECHAM4, only slight improvements are achieved with the new scheme. For example, the overestimated liquid water path and total cloud cover over convectively active regions are reduced in PCI. On the other hand, some shortcomings of the standard model such as underestimated shortwave cloud forcing over the extratropical oceans of the respective summer hemisphere are more pronounced in PCI.

1 Introduction

About 60% of the Earth's surface is covered with clouds. They are an important regulator of the Earth's radiation budget. For example, clouds cool the Earth-atmosphere system by 48 Wm^{-2} in the solar spectrum and warm it by 30 Wm^{-2} in the infrared as inferred from measurements of the Earth Radiation Budget Experiment (ERBE) (Collins et al. 1994). Additionally, clouds exert a major impact on the hydrological cycle and they affect the dynamics of the atmosphere through complex coupling among radiative, thermodynamic, and dynamic processes (Arakawa 1975). However, the lack of understanding of clouds remains one of the largest uncertainties in climate modeling and prediction (Gates 1992; IPCC 1992). The different treatment of cloud processes in general circulation models (GCMs) is still one of the main reasons for their differences in climate sensitivity (Cess et al. 1990).

Various parametrizations have been developed to represent clouds and their radiative effects in GCMs. The earliest approach uses a fixed geographical distribution of cloud fraction and cloud optical depth (e.g. Manabe et al. 1965; Boer et al. 1984). A more advanced method is to diagnose cloud cover from large-scale variables such as relative humidity (Smagorinsky 1960; Geleyn 1981) or additionally from vertical velocity, precipitation rate and strength of inversion (Slingo 1987). This approach has frequently been used in GCMs, e.g., Slingo (1987), McFarlane et al. (1992), Kiehl et al. (1994). The most recent trend in cloud parametrization is to obtain cloud water/ice from the respective transport equation following the pioneering work of Sundqvist (1978). In conjunction with that, cloud microphysical processes are parametrized at different levels of complexity. Although a physically based approach should in principle be preferred, the introduction of cloud microphysical processes which cannot be resolved on the spatial and temporal scales of a GCM introduces more complexity and more degrees of freedom. A prognostic scheme for cloud water and cloud ice together has been introduced, e.g., by Roeckner and Schlese (1985), LeTreut and Li (1988), Smith (1990), Del Genio et al. (1996). Cloud water and cloud ice are treated separately by Lee et al. (1992)

Correspondence to: U. Lohmann

This paper was presented at the Third International Conference on Modelling of Global Climate Change and Variability, held in Hamburg 4–9 Sept. 1995 under the auspices of the Max Planck Institute for Meteorology, Hamburg. Editor for these papers is L. Dümenil.

and Ose (1993). The most complex approach implemented in a GCM so far is given in Fowler et al. (1996), who use a prognostic scheme for cloud water, cloud ice, rain and snow. Further details about the different approaches and their realization in different GCMs can be found in Fowler et al. (1996).

In the current version of the Hamburg GCM (ECHAM4) only one prognostic equation for cloud water and cloud ice together is considered following Sundqvist (1978). Mixed cloud phase is always assumed between $-40\,°C$ and $0\,°C$ and the ratio of cloud water to cloud ice depends on temperature (Rockel et al. 1991). However, observational data show that the probability of occurrence of supercooled water clouds or pure ice clouds between $-40\,°C$ and $0\,°C$ is not negligible (Matveev 1984). Rangno and Hobbs (1994) show that cloud droplet size is a more reliable predictor than temperature of whether a cloud would glaciate. To allow for interactions between cloud droplets and ice crystals, the new approach considers cloud ice as a separate prognostic variable, in addition to water vapor and cloud water, similar to Lee et al. (1992), Ose (1993) and Fowler et al. (1996).

The three studies cited use parametrizations of the autoconversion rate of cloud droplets to rain drops which depend only on the liquid water content based on Kessler (1969) or Sundqvist (1978). However, cloud droplet spectra in maritime and continental clouds are very different. Aerosol particles such as sulfate aerosols, for example, can act as cloud condensation nuclei (CCN). The CCN spectrum and the water vapor supply in a cloud determine the cloud droplet number concentration (N_l). The characteristic of a typical continental cloud is a narrow droplet spectrum with many small droplets resulting from high levels of CCN. Maritime clouds typically have a broader spectrum with fewer and larger droplets, because fewer CCN are available (Pruppacher and Klett 1978). The precipitation formation in the warm phase depends mainly on the concentration of large droplets which is usually anticorrelated to N_l (e.g., Albrecht, 1989; Fouquart and Isaka 1992). Ship track observations reported by Radke et al. (1989) and King et al. (1993), for example, reveal a simultaneous increase in N_l and liquid water content of clouds compared to adjacent clouds. Thus the growth of large droplets by collision in clouds is suppressed in the track, so that the development of drizzle is prevented. Parametrizations which account for the dependence of the precipitation formation on N_l have been developed by e.g., Berry and Reinhardt (1973), Chen and Cotton (1987) and Beheng (1994).

Boucher et al. (1995) implemented a similar approach to Chen and Cotton (1987) in their GCM and investigated the amount of water stored in the atmosphere and the cloud radiative properties in relation to different prescribed values of N_l. We have introduced Beheng's (1994) parametrization of the autoconversion rate which is derived from the stochastic collection equation. Instead of prescribing N_l, we use empirical relationships between N_l and the sulfate aerosol mass (Boucher and Lohmann 1995), because sulfate aerosols are thought to be one of the dominant sources of CCN (e.g., Young 1993). A similar approach is taken for the conversion rate from cloud ice to snow by aggregation (Levkov et al. 1992). Unlike the parametrizations commonly used for the aggregation of ice crystals to snow (e.g., Kessler 1969; Rutledge and Hobbs 1983), the scheme of Levkov et al. (1992) avoids a threshold formulation and considers additionally the dependence on ice crystal size.

The new cloud microphysics scheme which has been developed to yield a more physically based representation of the components of the atmospheric moisture budget in the ECHAM model is described in Sect. 2. In addition, the changes in the cloud radiative properties are discussed. The effects of the cloud microphysics scheme on some hydrologic variables and on the radiation budget are analyzed in Sect. 3. A discussion and summary of the basic results in Sect. 4 concludes this study.

2 Model description

The dynamics and part of the model physics of the ECHAM model have been adopted from the European Centre for Medium-Range Weather Forecasts (ECMWF) model (Roeckner et al. 1992). Prognostic variables are vorticity, divergence, temperature, (logarithm of) surface pressure, and the mass mixing ratios of water vapor, and total cloud water (liquid and ice together). The model equations are solved on 19 vertical levels in a hybrid p-σ-system by using the spectral transform method with triangular truncation at wave number 30 (T30). Nonlinear terms and physical processes are evaluated at grid points of a "Gaussian grid" providing a nominal resolution of $3.75° \times 3.75°$. A semi-implicit leapfrog time integration scheme with $\Delta t = 30$ min is used for the simulation with T30 resolution.

Unlike previous versions, the current version employed for this study (ECHAM4) uses a semi-Lagrangian technique (Rasch and Williamson 1990) for computing the horizontal and vertical advection of positive definite quantities such as water vapor and total cloud water. As the semi-Lagrangian scheme is not mass conserving it cannot be applied to climate studies without a numerical mass fixer. Particularly in the case of strong vertical gradients the error in mass is extremely high resulting in an unrealistic transport. This problem is even more serious if cloud water and cloud ice are treated as separate prognostic variables. In addition, an analysis of the total cloud water budget equation (Roeckner, unpublished results) has shown that the advection term is more than an order of magnitude smaller than the respective sources and sinks (condensation and precipitation formation). For these reasons the advection of cloud water and cloud ice has been neglected in the new scheme (PCI).

Cumulus clouds are represented by a bulk model including the effects of entrainment and detrainment on the updraft and downdraft convective mass fluxes

(Tiedtke 1989). An adjustment closure based on the convective available potential energy (CAPE) is used (Nordeng 1994). Organized entrainment is assumed to depend on buoyancy, and the parametrization of organized detrainment is based upon a cloud population hypothesis. The turbulent transfer of momentum, heat, water vapor, and total cloud water is calculated on the basis of a higher order closure scheme (Brinkop and Roeckner 1995). The radiation code is based on a two-stream solution of the radiative transfer equation with six spectral intervals in the terrestrial infrared spectrum (Morcrette 1991) and two in the solar part of the spectrum (Fouquart and Bonnel 1980). Gaseous absorption due to water vapor, CO_2, O_3, CH_4, N_2O, and CFCs is included, as well as scattering and absorption due to prescribed aerosols and model-generated clouds. The cloud optical properties are described in Sect. 2.2. A new global set of land-surface parameters, including surface background albedo, surface roughness length, leaf area index, fractional vegetation cover, and forest ratio (Claussen et al. 1994) is used.

2.1 Cloud microphysics

In the new scheme the bulk microphysics parametrizations for warm phase processes are based mainly on Beheng (1994), while the parametrizations of the mixed and ice phase have been originally developed for a mesoscale model (Levkov et al. 1992). Since these parametrizations are necessarily scale-dependent some simplifications are required. The terminal velocity of cloud water as introduced in the pioneering work of Kessler (1969) is neglected. In contrast to ECHAM4 where the precipitation formation in the ice phase is parametrized in terms of the divergence of the cloud ice flux density, the terminal velocity of cloud ice is neglected in PCI. Following Ghan and Easter (1992) and Mölders et al. (1994), rain and snow are treated diagnostically. They find that by diagnosing rather than predicting rain and snow, the time step can be increased by a factor of ten with little loss in accuracy. Differences in form and structure of ice and snow crystals are neglected: "Pristine" non-aggregated ice particles and single snow crystals are assumed. The shapes of all hydrometeors are considered to be spherical. Sundqvist (1978) developed a formalism to include fractional cloud cover in a prognostic scheme. Its framework has been used in all ECHAM versions (Roeckner et al. 1992) and adopted in the new scheme as well. The governing equations for the mass mixing ratios of water vapor (q_v), cloud water (q_l) and cloud ice (q_i) in kg kg^{-1}, respectively, are:

$$\frac{\partial q_v}{\partial t} = R(q_v) - b(Q^c_{cnd} + Q^c_{dep}) + (1-b)(Q^o_{evp} + Q^o_{sub} - Q^o_{cnd} - Q^o_{dep}), \quad (1)$$

$$\frac{\partial q_l}{\partial t} = R(q_l) + b(Q^c_{cnd} - Q^c_{aut} - Q^c_{racl} - Q^c_{sacl} - Q^c_{frc} - Q^c_{frh} - Q^c_{frs} + Q^c_{mlt}) + (1-b)\,Q^o_{cnd}, \quad (2)$$

$$\frac{\partial q_i}{\partial t} = R(q_i) + b(Q^c_{dep} - Q^c_{agg} - Q^c_{saci} + Q^c_{frc} + Q^c_{frh} + Q^c_{frs} - Q^c_{mlt}) + (1-b)\,Q^o_{dep}, \quad (3)$$

where $R(...)$ denotes the sum over all transport terms of q_v, q_l, and q_i, respectively, including advection of water vapor, turbulence and convection (detrainment at the top of cumulus clouds) and b is the fractional cloud cover. The superscripts (c) and (o) refer to the cloudy and cloud-free part of the grid box, respectively. The cloud-microphysical processes simulated in the new scheme are condensation of water vapor and evaporation of cloud water in the cloudy part (Q^c_{cnd}), deposition of water vapor and sublimation of cloud ice in the cloudy part (Q^c_{dep}), evaporation of cloud water (Q^o_{cnd}) and sublimation of cloud ice (Q^o_{dep}) transported into the cloud-free part of a grid box, evaporation of rain (Q^o_{evp}), sublimation of snow (Q^o_{sub}), autoconversion of cloud droplets (Q^c_{aut}), accretion of cloud droplets by rain (Q^c_{racl}), by snow (Q^c_{sacl}), of ice crystals by snow (Q^c_{saci}), homogeneous (Q^c_{frh}), stochastical and heterogeneous (Q^c_{frs}), and contact freezing of cloud droplets (Q^c_{frc}), respectively, aggregation of ice crystals (Q^c_{agg}), and melting of cloud ice (Q^c_{mlt}). For simplicity the superscripts are omitted in the following.

Fractional cloud cover b is an empirical function of relative humidity (Sundqvist et al. 1989):

$$b = 1 - \sqrt{1 - b_o} \text{ with } b_o = (r - r_o)/(1 - r_o), \quad (4)$$

where r is the grid-mean relative humidity and r_o is a condensation threshold which is specified as a function of height following Xu and Krueger (1991). Condensational growth of cloud droplets or depositional growth of ice crystals occur if $r > r_o$. Conversely, an existing cloud is diluted by evaporation or sublimation if $r < r_o$. The moisture transported into a grid box with fractional cloud cover b is used partly for condensation or deposition and partly for moistening of the cloud-free area with b being the weighting factor (Sundqvist 1978). It is assumed that there are always sufficient condensation nuclei so that condensational growth is allowed to start as soon as the 100% relative humidity threshold in the cloudy part of the grid box is exceeded. Depositional growth of water vapor on ice crystals (Q_{dep}) always takes place at temperatures below $-35\,°C$. Above $-35\,°C$ Q_{dep} is a source for cloud ice only, if cloud ice is already present. Then saturation with respect to ice is assumed. Otherwise, water vapor condenses on cloud droplets at temperatures above $-35\,°C$. Cloud droplets can be transformed into ice crystals by stochastical, heterogeneous or contact freezing. In this case, saturation with respect to water is assumed.

The precipitation formation (autoconversion of cloud droplets) distinguishes between maritime and continental clouds by considering the cloud droplet number concentration (N_l) in addition to the liquid water content (Beheng 1994). It is derived from the stochastic collection equation, which describes the time evolution of a droplet spectrum changing by collisions among droplets of different size. The autoconversion rate Q_{aut} [kg kg^{-1} s^{-1}] in SI units is given by:

$$Q_{aut}=(\gamma_1 \cdot 6 \cdot 10^{28} n^{-1.7}(10^{-6}N_l)^{-3.3}(10^{-3}\ q_{cl})^{4.7})/\ , \quad (5)$$

where n ($=10$) is the width parameter of the initial cloud droplet spectrum, described by a Gamma function, is the air density and q_{cl} is the cloud water mixing ratio in the cloudy part of the grid box ($q_{cl}=q_l/b$). γ_1 ($=15$) is a microphysical constant which determines the efficiency of rain formation and, thus, the cloud lifetime. At present N_l cannot be computed realistically in GCMs because it depends on several factors which are not easy to predict, such as subgrid-scale velocity, maximum supersaturation, and availability of CCN. Therefore we empirically relate N_l to the sulfate aerosol mass (mSO_4^{2-}) (Boucher and Lohmann 1995). Monthly mean values of mSO_4^{2-} have been obtained from a sulfur cycle simulation with ECHAM (Feichter et al. 1996). Measurements of mSO_4^{2-}, CCN and N_l have been taken at various continental and marine sites in clean and polluted air, for a variety of weather situations. Hence, empirical relationships between N_l [m^{-3}] and mSO_4^{2-} [$\mu g\, m^{-3}$] can be derived for maritime and continental clouds:

$$N_l^{mar}=10^6 \cdot 10^{2.06+0.48\log(mSO_4^{2-})}. \quad (6)$$

$$N_l^{cont}=10^6 \cdot 10^{2.24+0.257\log(mSO_4^{2-})}. \quad (7)$$

Figure 1 shows the geographical distribution of N_l in model level 15 (approximately 850 hPa) for January and July, respectively. Maxima in N_l are associated with high sulfur emissions due to industrial activity in North America, Europe and Southeast Asia. Secondary maxima in the Southern Hemisphere are caused by biomass burning. The concentrations over remote oceanic regions range between 25 and 75 droplets cm^{-3}. High levels of mSO_4^{2-} are transported downwind of the industrial centers off the shores of the Asian and North American coast, yielding high concentrations of N_l. In July mSO_4^{2-} and, hence, N_l over the Northern Hemisphere is higher, because more oxidants are available to form sulfate aerosols and fewer sulfate aerosols are washed and rained out (Feichter et al. 1996).

Raindrops, once formed, continue to grow by accretion of cloud water. The accretion rate is derived from the stochastic collection equation (Beheng 1994):

$$Q_{racl}=a_1 \cdot \ \cdot q_{cl} \cdot q_r, \quad (8)$$

where q_r is the rainwater mixing ratio and $a_1=6\ s^{-1}$.

At temperatures below $-35\,°C$ the total amount of cloud water freezes homogeneously and instantaneously to cloud ice (Lord et al. 1984; Eppel et al. 1995):

$$Q_{frh}=q_{cl}/\Delta t. \quad (9)$$

For stochastical and heterogeneous freezing of cloud droplets between $0\,°C$ and $-35\,°C$ we use the extrapolated Bigg's (1953) equation down to the cloud droplet size (Levkov et al. 1992; Murakami 1990):

$$Q_{frs}=a_2\{\exp[b_2(T_o-T)]-1\}\frac{q_{cl}^2}{{}_lN_l}, \quad (10)$$

where a_2 ($=100\ m^{-3}s^{-1}$) and b_2 ($=0.66\ K^{-1}$) are determined from laboratory experiments. ${}_l$ ($=1000$ $kg\, m^{-3}$) is the density of water, T the grid-mean temperature and $T_o=273.16$ K.

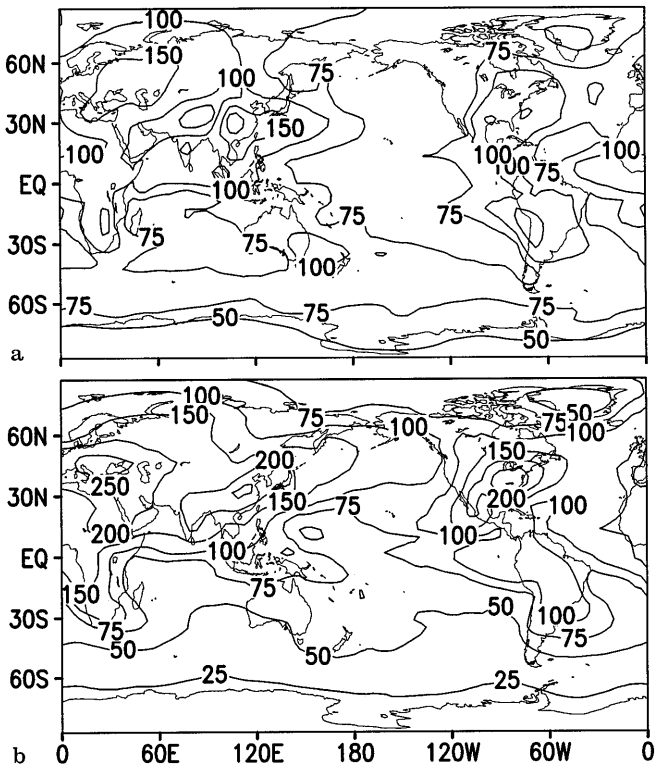

Fig. 1a, b. Cloud droplet number concentration for January (*upper panel*) and July (*lower panel*). Contour spacing: 25, 50, 75, 100, 150, 200, 250, 300 cm^{-3}

Brownian-diffusion contact nucleation results from random collision of aerosol particles with supercooled cloud droplets. It may be written as (Levkov et al. 1992; Cotton et al. 1986):

$$Q_{frc}=m_{io}F_1DF_{ar}, \quad (11)$$

where DF_{ar} ($=1.4*10^{-8}\ m^{-2}s^{-1}$) is the aerosol diffusivity (Pruppacher and Klett 1978), m_{io} ($=10^{-12}$ kg) is the initial mass of a nucleated ice crystal, and

$$F_1=4\pi r_{lv}N_lN_a/\ . \quad (12)$$

The concentration of active contact nuclei is approximated to $N_a=N_{ao}\,(270.15-T)$, with $N_{ao}=2*10^5\ m^{-3}$. r_{lv} is the mean volume cloud droplet radius:

$$r_{lv}=\sqrt[3]{\frac{3q_{cl}}{4\pi\ {}_lN_l}}. \quad (13)$$

The conversion rate from cloud ice to snow by aggregation of ice crystals according to Levkov et al. (1992) based on work of Murakami (1990) is given by:

$$Q_{agg}=\gamma_2 q_{ci}/\Delta t_1, \quad (14)$$

where q_{ci} is the cloud ice mixing ratio in the cloudy part of the grid box ($q_{ci}=q_i/b$), γ_2 ($=220$) is again a microphysical constant which determines the efficiency of snow formation and, thus, the ice cloud lifetime and Δt_1 is equal to the time needed for the ice crystal number concentration to decrease from N_i to $N_i(r_{iv}/r_{so})^3$:

$$\Delta t_1 = -\frac{2}{c_1}\log\left(\frac{r_{iv}}{r_{so}}\right)^3. \quad (15)$$

r_{so} ($=10^{-4}$ m) is the smallest radius of a particle in the snow class and

$$c_1 = \frac{q_{ci}\ a_3 E_{ii} X}{i}\left(\frac{}{o}\right)^{0.33}, \quad (16)$$

with X ($=0.25$) is the dispersion of the fall velocity spectrum of cloud ice, E_{ii} ($=0.1$) is the collection efficiency between ice crystals, $_o$ ($=1.3$ kg m^{-3}) is the air density at the surface, $_i$ ($=500$ kg m^{-3}) is the density of cloud ice, a_3 ($=700$ s^{-1}) is an empirical constant (Murakami 1990), and r_{iv} is the mean volume ice crystal radius (see Sect. 2.2).

The parametrization of the accretional growth of snow (riming and collecting ice crystals) according to Levkov et al. (1992) is based on Lin et al. (1983). Snow crystals are assumed to be distributed exponentially (Gunn and Marshall 1958):

$$n_s(D_s) = n_{os}\exp(-\lambda_s D_s), \quad (17)$$

where $n_s(D_s)$ is the concentration of particles of diameter D_s per unit size interval. D_s is the diameter of the water drop formed by the melting snow particle. n_{os} ($=3*10^6$ m^{-4}) is the intercept parameter obtained from measurements (Gunn and Marshall 1958). λ_s is the slope of the particle size distribution and is written as (Potter 1991):

$$\lambda_s = \left(\frac{\pi\ _l n_{os}}{q_s}\right)^{0.25}, \quad (18)$$

where q_s is the snow mixing ratio. Snow crystals settle through a population of supercooled cloud droplets, colliding and coalescing with them (riming). The rate of change in the mixing ratio for snow is based on the geometric sweep-out concept integrated over all snow sizes for the assumed snow size distribution given in Eq. (17):

$$Q_{sacl} = \gamma_3 \frac{\pi E_{sl} n_{os} a_6 q_{cl} \Gamma(3+b_6)}{4\lambda_s^{3+b_6}}\left(\frac{}{o}\right)^{0.5}, \quad (19)$$

where $a_6 = 4.83$, $b_6 = 0.25$. E_{sl} ($=1$) is the collection efficiency of snow for cloud droplets (Lin et al. 1983). Levkov et al. (1992) limited the riming process to cloud water mixing ratios $\geq 10^{-5}$ kg kg^{-1}. Instead of this, we have chosen γ_3 ($=0.1$).

The accretion rate of ice crystals by snow is similar to Eq. (19) and is expressed as:

$$Q_{saci} = \frac{\pi E_{si} n_{os} a_6 q_{ci} \Gamma(3+b_6)}{4\lambda_s^{3+b_6}}\left(\frac{}{o}\right)^{0.5}. \quad (20)$$

The collection efficiency of snow for cloud ice (E_{si}) is assumed to be temperature dependent:

$$E_{si} = \exp(0.025(T - T_o)). \quad (21)$$

All ice crystals melt immediately when the temperature is above 0 °C (Fowler et al. 1996):

$$Q_{mlt} = q_{ci}/\Delta t. \quad (22)$$

The rain formed is then given by the sum of Eqs. (5) and (8) and the snow formed by the sum of Eqs. (14), (19) and (20).

Rain falling into the cloud-free part of a grid box is exposed to evaporation, which is parametrized in terms of the saturation deficit (Roeckner et al. 1992):

$$Q_{evp} = -\frac{1}{\Delta t}\frac{\gamma_4(q_v - q_{vs})}{1 + \frac{L_v}{c_p}\frac{dq_{vs}}{dT}}, \quad (23)$$

where γ_4 ($=0.15$) is a tunable parameter. q_{vs} is the saturation water vapor, L_v ($=2.5008*10^6$ J kg^{-1}) the latent heat of vaporization and c_p is the specific heat of moist air at constant pressure. Similarly, sublimation of snow is expressed as:

$$Q_{sub} = -\frac{1}{\Delta t}\frac{\gamma_4(q_v - q_{vs})}{1 + \frac{L_s}{c_p}\frac{dq_{vs}}{dT}}, \quad (24)$$

where L_s ($=2.8345*10^6$ J kg^{-1}) is the latent heat of sublimation.

Melting of snow occurs when the temperature exceeds 2 °C based on observational data by Mason (1971). It is not only limited by the snow amount, but also by keeping the cooling of the layer linked to this, such that the temperature of the layer after melting is not lower than 2 °C (Roeckner et al. 1992).

2.2 Cloud radiative properties

As in ECHAM4, the radiative properties of water droplets and approximately "equivalent" ice crystals are derived from Mie theory, and the results are fitted to the spectral resolution of the radiation model and formulated in terms of cloud droplet and ice crystal effective radii (Rockel et al. 1991). In order to account for the non-sphericity of ice crystals, the asymmetry factor has been empirically reduced to ~ 0.8 for a wide range of effective ice radii. For liquid clouds, the mean volume cloud droplet radius (r_{lv}) is calculated according to Eq. (13) from the liquid water content in the cloudy part of the grid box and the cloud droplet number concentration (N_l) as defined in Eqs. (6) and (7). Note that unlike PCI an idealized distribution of N_l is used in ECHAM4 (Roeckner 1995) assuming different values for continental clouds ($N_l = 220$ cm^{-3}) and maritime clouds ($N_l = 100$ cm^{-3}) in the planetary boundary layer with a gradual reduction down to $N_l = 50$ cm^{-3} in the upper model layers.

Simultaneous measurements of r_{lv} and the effective radius of cloud droplets (r_{le}) suggest a linear regression between the two radii:

$$r_{le} = k\, r_{lv}, \quad (25)$$

with $k = 1.143$ for continental clouds and $k = 1.077$ for maritime clouds (Johnson 1993). Moss et al. (submitted 1996) derived an empirical relationship between the effective radius (r_{ie} [m]) of an ice crystal distribu-

tion and the ice water content based on aircraft observations of frontal clouds around the British Isles:

$$r_{ie} = a_4 * 10^{-6} (10^3 \quad q_{ci})^{b_4}, \tag{26}$$

where $a_4 = 83.8$ and $b_4 = 0.216$.

From simultaneous measurements of r_{ie} and r_{iv} Moss et al. (submitted 1996) derived a quadratic relationship between the two:

$$r_{ie} = 10^{-6} \cdot \sqrt[3]{a_5 (10^6 r_{iv})^3 + b_5 (10^6 r_{iv})^6}, \tag{27}$$

where $a_5 = 1.61$ and $b_5 = 3.56 * 10^{-4}$.

3 Results

The results presented are based on 5-year integrations at T30 resolution using the standard cloud scheme of ECHAM4 and the prognostic cloud ice scheme (PCI), respectively. The model is forced by observed sea surface temperatures and sea ice extents for the period 1985–1989 taken from the Atmospheric Model Intercomparison Project (AMIP) data set (Gates 1992).

3.1 Global means

Table 1 shows a comparison of globally averaged values of different components of the hydrologic cycle and of the cloud radiative forcing for January and July, respectively. The values represent ensemble averages over the whole observed and simulated period. Note that the time span for the different data sets is not the same. The integration period agrees with the period of ERBE measurements, but is different from the periods for which the observed climatologies of liquid water path (LWP: 1987–1994 according to Weng and Grody 1994 and 1987–1991 according to Greenwald et al. 1993) and water vapor mass (WVM: 1987–1988 according to Ewald and Schluessel in preparation 1996) have been compiled. This might explain some of the differences between model and observations. On a global scale, the only data sets of cloud water and cloud ice available so far are distributions of LWP derived from microwave emissions over ice-free oceans (e.g. Greenwald et al. 1993; Weng and Grody 1994). Yet, the accuracy is still rather low, and the retrievals can be affected by many input factors (e.g., total precipitable water, surface wind, cloud temperature). There are also possible contributions from precipitation-size drops in the retrieved LWP. Hence, the retrievals from Greenwald et al. (1993) and Weng and Grody (1994) differ regionally by a factor of two. We use both data sets as an estimate of the possible range of LWP. Both simulations lie within the observed range, closer to the upper value as retrieved by Greenwald et al. (1993).

The largest differences between the simulations occur in the ice water path. The total amount in PCI is 33% (24%) higher in January (July) than in ECHAM4. The ensemble mean of globally averaged total cloud cover (TCC) in PCI is 64% and 60% for January and July, respectively. It differs insignificantly from the 62% for January and July as derived from the International Satellite Cloud Climatology Project (ISCCP; Rossow and Schiffer 1991) and from surface observations (Hahn et al. 1994). The global means of water vapor mass are slightly higher in PCI as compared to ECHAM4 and to the retrieved values from SSM/I (Ewald and Schluessel in preparation 1996). Total precipitation is 7% lower in PCI than in CTL and the ratio between convective and large-scale precipitation is different. While in ECHAM4 53% of the global annual mean total precipitation originates from large-scale clouds this fraction reduces to 42% in PCI as a result of a higher evaporation and sublimation rate of stratiform precipitation in PCI.

The impact of clouds on the top-of-atmosphere (TOA) radiation balance is most conveniently de-

Table 1. Globally averaged values of water vapor mass (WVM), liquid water path (LWP), ice water path (IWP), total cloud cover (TCC), shortwave (SCF) and longwave (LCF) cloud forcing from model simulations (ECHAM4 and PCI) and observations, for January and July

		Observations		ECHAM4		PCI	
		Jan	Jul	Jan	Jul	Jan	Jul
WVM ($kg\ m^{-2}$)	SSM/I (Ewald and Schlüssel in preparation 1996)	29	29	29	30	31	31
LWP ($g\ m^{-2}$)	SSM/I (Greenwald et al. 1993)	78	84	78	80	80	77
	SSM/I (Weng and Grody 1994)	51	53				
IWP ($g\ m^{-2}$)				18	21	24	26
TCC (%)	ISCCP	62	62	64	60	64	60
	Surface observations (Hahn et al. 1994)	62	62				
SCF ($W\ m^{-2}$)	ERBE	−52	−48	−55	−49	−51	−45
LCF ($W\ m^{-2}$)	ERBE	29	29	27	29	29	30

Note that global values of WVM, LWP and IWP are restricted to oceans between 60°S and 60°N. Uncertainties of the observations are estimated to be 5 Wm^{-2} for ERBE, 4.4 $kg\ m^{-2}$ for individual measurements of WVM, 5% regional bias (higher in polar regions) for ISCCP, and the two estimations of LWP suggest an uncertainty of about 60%

scribed by the cloud radiative forcing (CF). Following Ramanathan et al. (1989) CF is defined in terms of the emitted longwave radiation F, the solar irradiance S_o, and the albedo α according to:

$$CF = LCF + SCF = (F_{cs} - F) - S_0(\alpha - \alpha_{cs}), \quad (28)$$

where the subscript *cs* is used for clear-sky quantities and *LCF* and *SCF* represent the longwave and shortwave components of *CF,* respectively. The global annual mean *SCF* and *LCF* in PCI have been tuned to roughly match the ERBE data by an appropriate choice of the microphysical constants which determine the mean lifetime of the clouds (γ_1 to γ_4 in Sect. 2.1). Both simulations show some skill in reproducing the seasonal variations of the shortwave component. Even the largest differences of about 3 Wm^{-2} are probably within the range of observational uncertainty.

3.2 Geographical distribution of cloud water, cloud ice and cloud cover

Figure 2 shows the annual mean latitude-height cross sections of cloud water and cloud ice for ECHAM4 and PCI, respectively, and the differences in cloud water and cloud ice between both simulations. For ECHAM4 the separation between cloud water and cloud ice is calculated off-line. Cloud water has maxima in the lower troposphere associated with tropical shallow convection and extratropical cyclones in both hemispheres and experiments. Note that one shortcoming of ECHAM4, namely too high values of cloud water near the surface, is reduced in PCI. In the extratropics cloud water has shifted into higher altitudes, while it has decreased in the midtroposphere of the tropics. Major differences occur in cloud ice. The largest increase in cloud ice in PCI as compared with ECHAM4 can be seen in the middle and upper troposphere of the extratropics. In the tropics cloud ice has slightly decreased and has been shifted into higher altitudes. Secondary maxima in cloud ice occur in the lower troposphere of midlatitudes. This is caused by a rapid growth of ice crystals by stochastic freezing and contact freezing of cloud droplets and subsequent deposition of water vapor on ice crystals. The aggregation of ice crystals increases with increasing ice crystal size. Additionally the collection efficiency of snow flakes with ice crystals increases with temperature according to Eq. (21), so that the conversion from ice crystals to snow is the faster the warmer the atmosphere is and the larger the crystals are. Therefore long-lived ice clouds are restricted to colder temperatures, i.e., higher altitudes as compared to ECHAM4.

Figures 3 and 4 present the geographical distributions of the LWP for ensemble means of January and July, respectively. ECHAM4 and PCI are able to capture the observed maxima in LWP associated with tropical convection and extratropical cyclones in the Northern Hemisphere in January, but both simulations underpredict LWP over the Southern Hemisphere oceans with respect to the retrieval of Greenwald et al. (1993). In PCI the overestimation of LWP in convectively active regions, e.g., in the intertropical convergence zone (ITCZ), the South Pacific convergence zone (SPCZ), and in the Indian Ocean is less apparent than in ECHAM4. Due to high levels of sulfate aero-

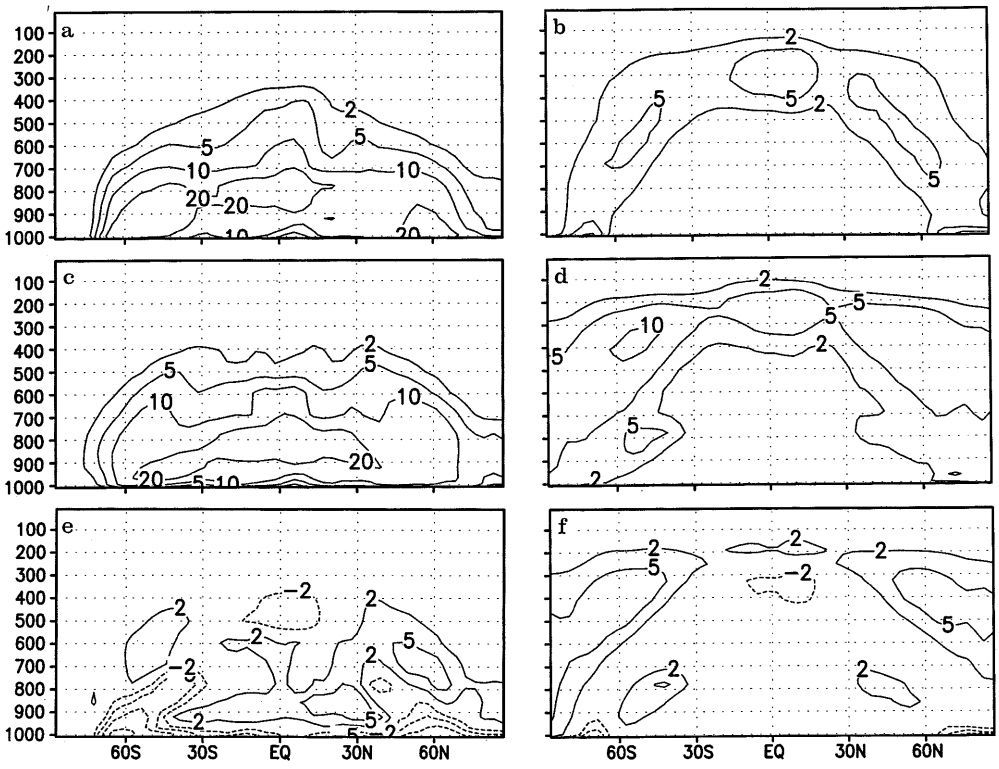

Fig. 2a–f. Annual mean latitude-height cross sections of cloud water and cloud ice for ECHAM4 **a, b** and PCI **c, d**, respectively, and the differences in cloud water and cloud ice between PCI and ECHAM4 **e, f**, respectively. Contour spacing: ± 2, ± 5, ± 10, ± 20, $\pm 50 * 10^{-6} kg^{-1}$

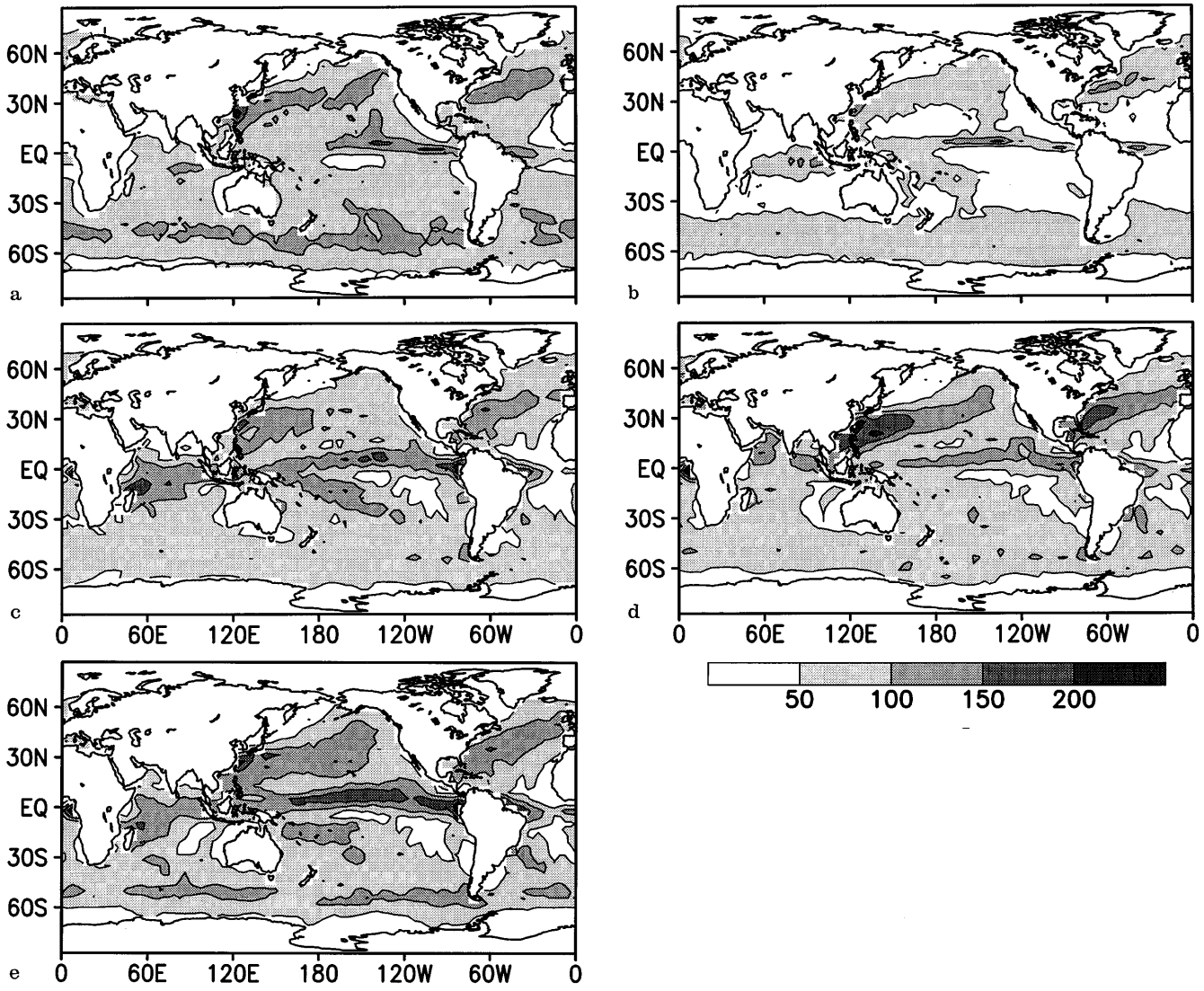

Fig. 3a–e. Geographical distribution of liquid water path for January obtained from SSM/I analyses **a** according to Greenwald et al. (1993); **b** SSM/I analyses according to Weng and Grody (1994); **c** ECHAM4; **d** PCI; **e** a sensitivity experiment using PCI with constant, but different values of N_l over land and ocean (see text). Contour spacing is 50 g m^{-2}

sols and, hence, high concentration of cloud droplets (cf. Fig. 1), higher values of LWP as observed are predicted over the western part of the North Atlantic and North Pacific, respectively. However, Liu and Curry (submitted 1995) derived LWP from SSM/I for January 1993 with values over 300 g m^{-2} off the west coast of North America, which exceeds both other retrievals and the high values in PCI. In July the maxima of LWP associated with extratropical cyclones are much more pronounced over Northern Hemisphere oceans than over Southern Hemisphere oceans as suggested from SSM/I (Fig. 4). This feature hardly shows up in ECHAM4, but is indicated in PCI, although the maxima are further south than observed.

The differences in the simulated LWP can be caused by a variety of model changes, such as (1) the different power of q_{cl} in the autoconversion rate, (2) the introduction of spatial variations in N_l or (3) the different parametrizations of mixed-phase processes, like freezing or riming. In order to get some insight into the importance of these processes, additional sensitivity experiments have been carried out. In the first one, the spatial variation of N_l is limited to land-ocean differences, analogous to ECHAM4. For this experiment, average values of N_l in the planetary boundary layer have been derived from PCI over land (N_l=135 cm^{-1}) and ocean (N_l=80 cm^{-1}), respectively. With respect to PCI, LWP increases by 10% over the oceans as a result of larger N_l in regions with large cloudiness and low sulfate in PCI, like the Southern Hemisphere oceans or the ITCZ (cf. Fig. 1). The distribution of LWP approaches that of ECHAM4 (Fig. 3e versus Fig. 3c, d), most notably in the tropics, where the larger N_l leads to larger LWP as compared to PCI. Conversely, N_l over the western part of the North Pacific and North Atlantic is lower in this experiment yielding a smaller LWP than in PCI, closer to that of ECHAM4. In a second sensitivity experiment, where ECHAM4

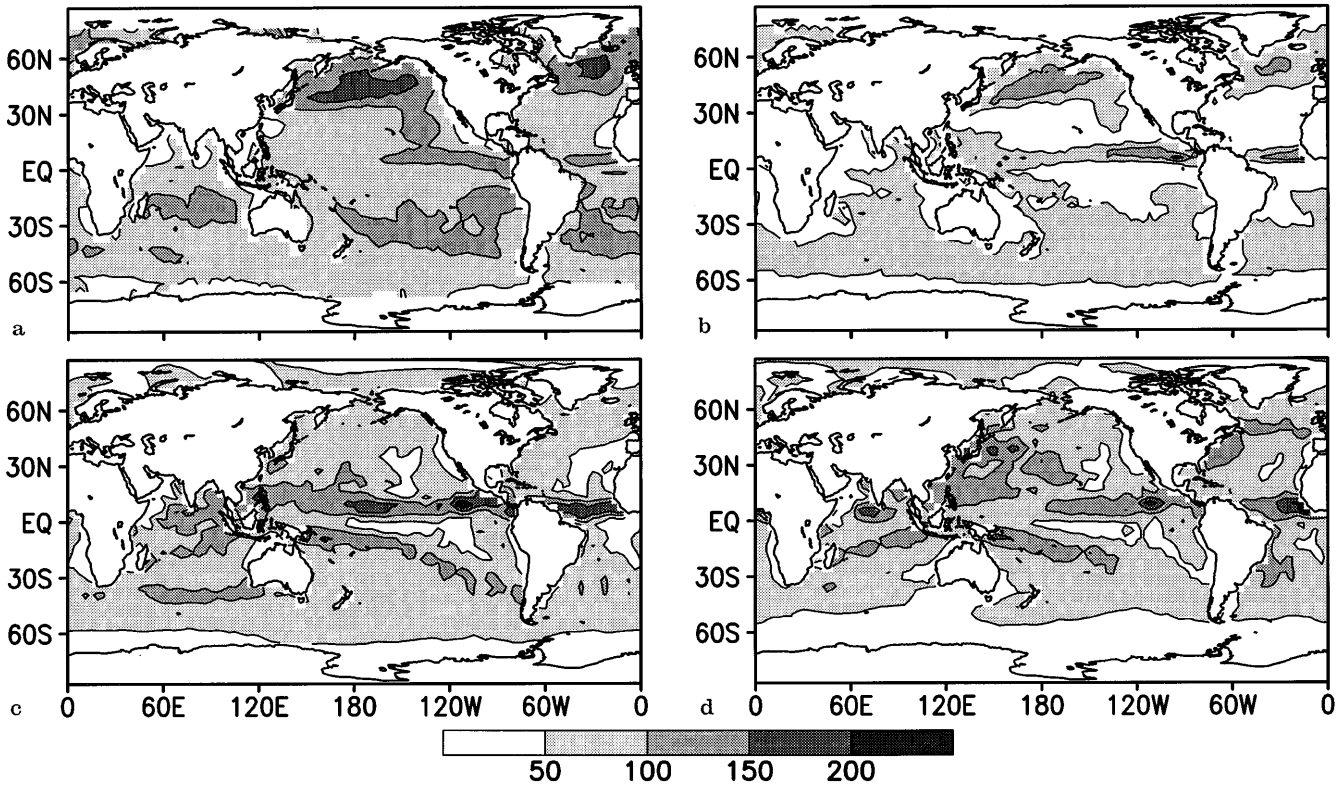

Fig. 4a–d. As Fig. 3a–d except for July

was used with the warm cloud physics of PCI including the empirical relationships between N_l and mSO_4^{2-}, the distribution of LWP approaches the one in PCI, which confirms the results of the first experiment (not shown). To conclude, the introduction of spatial variations in N_l has the strongest impact on LWP, while the treatment of mixed-phase processes is of secondary importance.

Satellite retrievals of cloud ice are not yet available, so the only data sets that can be used for model validation are those obtained during field campaigns (e.g. FIRE, ICE, CEPEX). Figure 5 shows the average ice water content (IWC) versus in-cloud temperature measured by aircraft (Learjet) during the Central Equatorial Pacific Experiment (CEPEX) between 20°S and 2°N, and between 165°E and 170°W (Lohmann et al. 1995; McFarquhar and Heymsfield 1996). Vertical bars indicate the 25% and 75% quartiles of the observations. The simulated IWC of ECHAM4 and PCI within the same domain is taken for respective March ensembles. The average IWC is dominated by a few cases with large IWCs, because the IWC in each temperature bin is positively skewed. It can, therefore, exceed the 75% percentile value (Fig. 5). Since the Learjet data probably include supercooled cloud droplets, the sum of cloud ice and supercooled cloud water is taken from the model simulations for the comparison. Both simulations capture the observed increase of IWC with temperature. The IWC in PCI deviates more from the observed one than in ECHAM4 for temperatures above 230 K, but it still lies between the observed 25% and 75% quartiles. Although the IWC has increased globally in PCI (cf. Table 1), it is lower than in ECHAM4 for temperatures above 230 K. However, according to Fig. 2, the tropical IWC has slightly decreased in PCI and has been shifted to higher altitudes, and, thus colder temperatures which is reflected in Fig. 5. Due to the

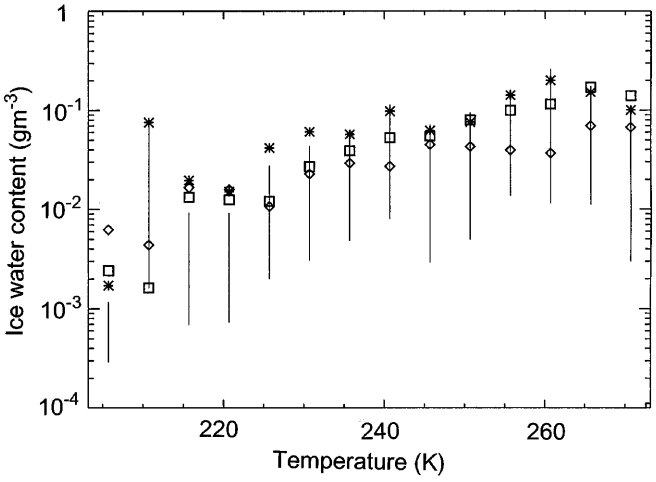

Fig. 5. Mean ice water content versus in-cloud temperature in 5 K temperature bins from 2DC-probe data carried on the Aeromet Learjet (*stars*) during CEPEX as compared to ECHAM4 (*squares*) and PCI (*rhombs*). *Vertical bars* represent the 25% and

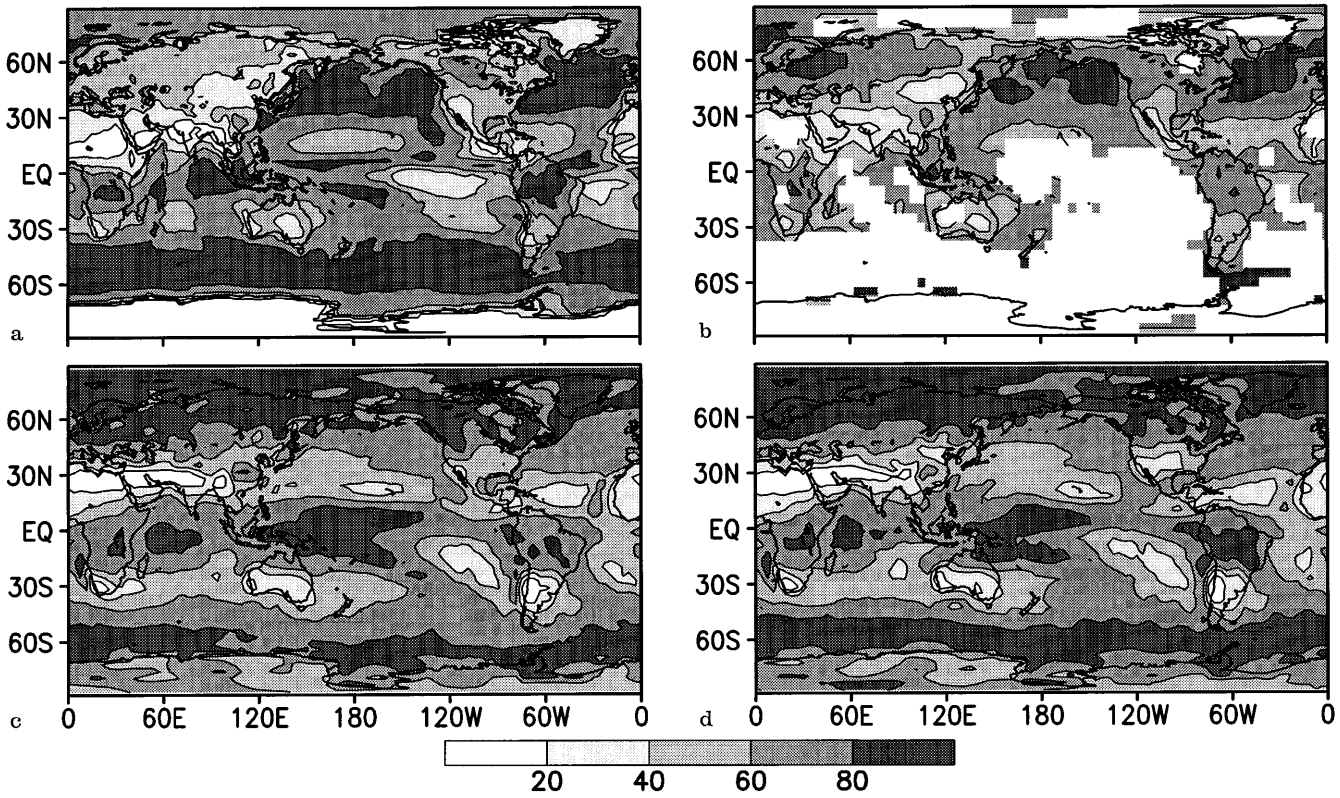

Fig. 6a–d. Geographical distribution of cloud cover for January obtained from **a** ISCCP; **b** surface observations (Hahn et al. 1994); **c** ECHAM4 and **d** PCI. Contour spacing is 20%

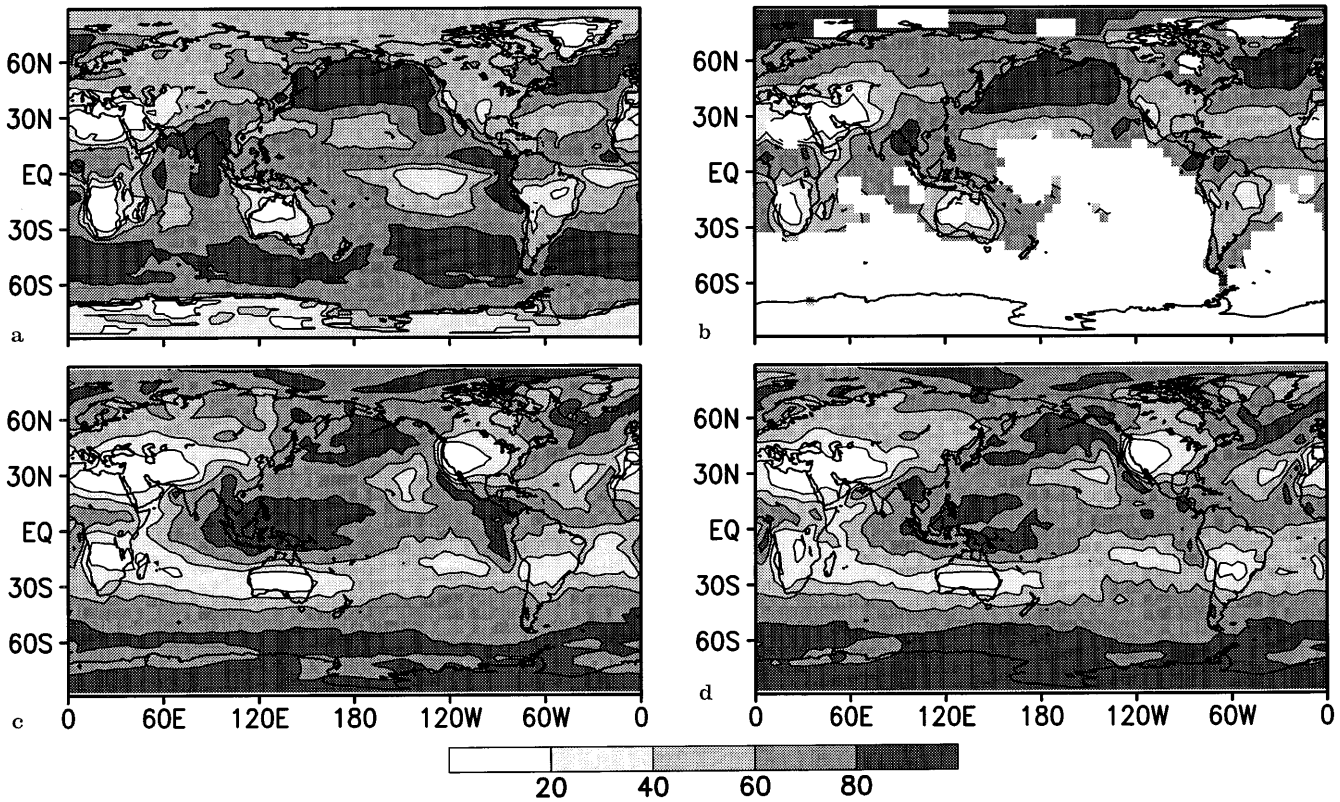

Fig. 7a–d. As Fig. 6 except for July

coarser resolution in the model, extreme values of IWC will hardly appear in the results. The 5% and 95% values in ECHAM4 and PCI have a smaller range than observed. Hence, the variability within each temperature bin is underestimated in both simulations. However, the range of cloud ice alone in PCI can exceed the range of the sum of supercooled cloud water and cloud ice by a factor of 30 and, thus, can reach approximately the observed range of four orders of magnitude (not shown).

Figures 6 and 7 show the geographical distribution of TCC of ensemble means for January and July, respectively. Note that a very limited amount of data over the oceans is available from the surface observations (Hahn et al. 1994). Both observed data sets agree very well, except over the Northern Hemisphere continents where the satellite observations tend to underpredict TCC by 10% (Rossow et al. 1993). Maxima in TCC, associated with tropical convection and extratropical cyclones, are captured in both simulations and months. In January both simulations underpredict TCC over the Northern Hemisphere oceans and overpredict it over Northern Hemisphere continents, even with regard to the surface observations. In ECHAM4 and PCI the cloud amount of marine stratocumulus decks off the Californian coast is too low, which is a characteristic of many numerical models, and has been attributed to insufficient vertical resolution in the planetary boundary layer. In July (Fig. 7) both simulations underpredict TCC over the storm tracks of the Northern Hemisphere, but capture high values of TCC associated with the Asian summer monsoon. The overestimation of TCC over tropical convectively active systems is reduced in PCI as compared to ECHAM4 in both months.

3.3 Geographical distribution of cloud radiative forcing

So far we have discussed the main parameters determining the cloud radiative processes (cloud water, cloud ice and cloud cover). It has been shown that the simulated quantities agree reasonably well with the observed ones. Next the simulated SCF and LCF will be compared to the observed ones from ERBE. Figures 8 and 9 present ensemble mean SCF for January and July, respectively. In January the maximum SCF occurs over the Southern Hemispheric oceans with values up to $-200\,\mathrm{Wm}^{-2}$. Secondary maxima are associated with tropical convection. Both simulations capture the overall features but underestimate SCF over the Southern Hemispheric oceans. In July (Fig. 9) the maximum SCF has moved to Northern Hemispheric oceans following the seasonal cycle of insolation. High values of SCF are also linked to the Asian summer monsoon and to marine stratocumulus decks off the coasts of California and South America. ECHAM4 and PCI simulate the gross features but differ in the details. SCF over the storm tracks is underestimated as a result of underpredicted TCC and LWP (cf. Figs. 3–4 and Figs. 6–7 and Chen and Roeckner 1996). The spatial extent of secondary maxima associated with marine stratocumulus is too small in both simulations, as a result of too little TCC. In both seasons the overestimation of SCF associated with tropical convection is reduced in PCI, which is attributable to the lower values of LWP over convectively active regions. Yet, SCF is too high over oceanic subsidence regions in both experiments.

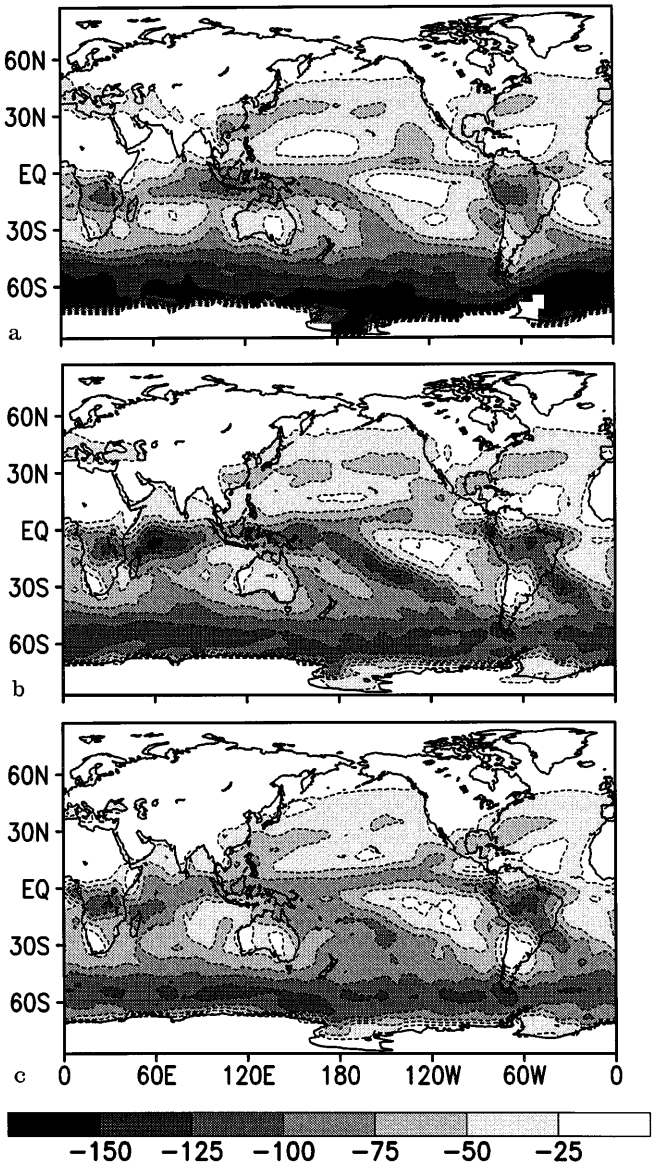

Fig. 8a–c. Geographical distribution of shortwave cloud forcing for January obtained from **a** ERBE, **b** ECHAM4 and **c** PCI. Contour spacing is 25 Wm^{-2}

Finally, ensemble means of LCF for January and July are displayed in Figs. 10 and 11, respectively. In contrast to SCF which is mainly determined by the presence of water clouds, LCF is strongly related to the presence of ice clouds. Both ECHAM4 and PCI simulate the location and seasonal shift of high LCF over

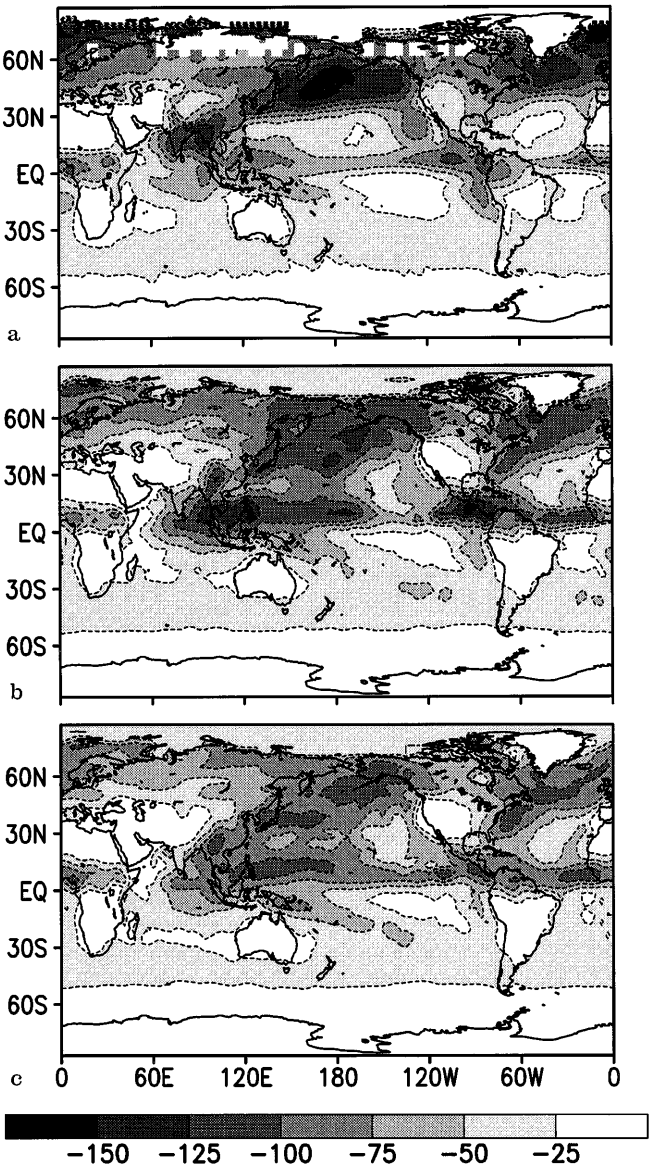

Fig. 9a–c. As Fig. 8 except for July

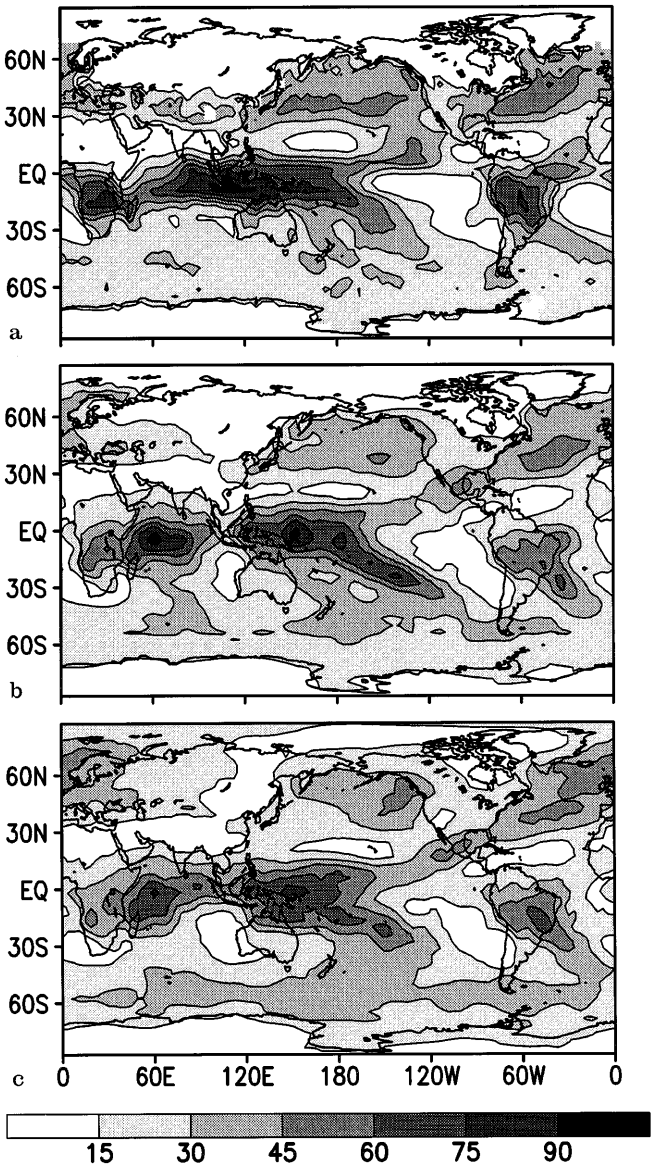

Fig. 10a–c. Geographical distribution of longwave cloud forcing for January obtained from **a** ERBE, **b** ECHAM4 and **c** PCI. Contour spacing is 15 Wm^{-2}

the tropics reasonably well. Due to the occurrence of cloud ice in higher altitudes in the extratropics in PCI as compared to ECHAM4, LCF is larger than observed over the Southern Hemisphere oceans in January. Instead of one coherent band of convective activity reaching from the Indian Ocean via Indonesia to the mid-Pacific in January, two distinct centers are simulated in ECHAM4. PCI simulates one coherent band with too low peak values. In July (Fig. 11) the Pacific ITCZ is distinctly marked in ERBE. In ECHAM4 it is not as coherent as ERBE indicates and LCF over Indonesia and Central America is overestimated. This is caused by an excessively strong Walker circulation (Chen and Roeckner 1996). In PCI the Pacific ITCZ is slightly better represented but not as pronounced as in the ERBE data. On the other hand, the peak values of LCF over convectively active regions are close to the observed ones, and the Walker circulation is less excessive than in ECHAM4.

4 Discussion and summary

First results obtained from a new cloud microphysics scheme including a prognostic treatment of cloud ice (PCI) in the general circulation model ECHAM are presented. In contrast to the standard scheme of ECHAM4, the autoconversion from cloud water to rain depends additionally on the cloud droplet number concentration (N_l) to account for the different micro-

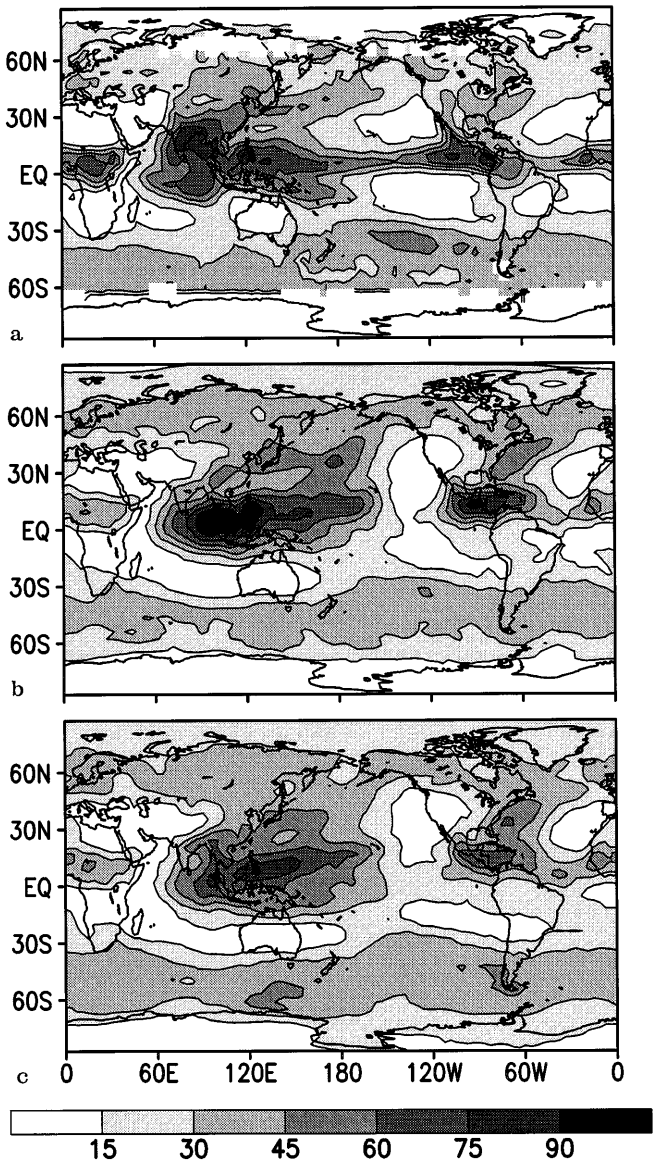

Fig. 11a–c. As Fig. 10 except for July

physical properties of maritime and continental clouds. N_l is empirically related to the sulfate aerosol mass. Similarly, the aggregation of ice crystals to snow depends additionally on the ice crystal size, which is a function of the ice water content. The vertical distribution of cloud ice differs remarkably between the two schemes. While ECHAM4 always assumes mixed clouds between $-40\,°C$ and $0\,°C$, in PCI supercooled water clouds can exist down to $-35\,°C$ and pure ice clouds up to $0\,°C$. Once glaciation of these clouds starts, the subsequent precipitation formation is more efficient for larger ice crystals. Additionally the accretion of snow flakes with ice crystals is more efficient for higher temperatures. Therefore maxima in ice water content in PCI are confined to higher altitudes and the ice water path is 33% and 24% higher in January and July, respectively, than in ECHAM4.

In general, the simulated distributions of cloud water and cloud ice with ECHAM4 and with PCI are within the range of the observational uncertainty which is unfortunately very high. The climatology of cloud physical and radiative properties is reasonably well simulated with ECHAM4. Therefore only minor improvements are achieved with PCI, e.g., the overestimation of LWP and TCC in convectively active regions is reduced. This is caused by the low concentration of N_l in those clouds (cf. Fig. 1) and therefore a fast precipitation formation.

However, some shortcomings like the overprediction of LWP off the Asian coast compared to the microwave retrievals of LWP from Greenwald et al. (1993) and Weng and Grody (1994) due to high values of N_l occur. Here we have taken a simple empirical approach to relate N_l to the monthly mean values of sulfate aerosol mass (mSO_4^{2-}), because sulfate aerosols are one of the major contributors to cloud condensation nuclei (CCN) (e.g., Young 1993). However, nitrates and organic species are locally at least as important as sulfate in acting as CCN (Novakov and Penner 1993; Malm et al. 1994), whereas sea salt aerosols are believed to make only a small contribution to the total CCN number in remote marine areas (Fouquart and Isaka 1992) and over the east coast of the United States (Hegg et al. 1995). Applying a relationship between N_l and mSO_4^{2-} further implies a constant fraction of mSO_4^{2-} to the total aerosol mass, which is definitely not what has been observed. The fraction of mSO_4^{2-} to the total aerosol mass ranges from 14% to 69% over the United States (Malm et al. 1994), from 20% to 100% over the east coast of the United States (Hegg et al. 1995), and from 23% for maritime aerosols over the Atlantic to 22%–45% for continental aerosols and further to 75% in the Arctic region (Warneck 1988). Even though Hegg et al. (1995) find that the fraction of mSO_4^{2-} to the total mass of accumulation mode particles is on average 62%, they conclude that in their limited data set most of the CCN were not sulfate. Nevertheless our approach is justified as sulfate aerosols are the best explored aerosols on a global scale. Up to now no global distributions of nitrate or organic aerosols exist, so our relationship between N_l and mSO_4^{2-} is a first step in coupling aerosols and N_l. Since a realistic aerosol size distribution should be considered and sensitivity experiments (cf. Fig. 3) have shown that the distribution of LWP depends strongly on N_l, the coupling of N_l to aerosol physics should be further pursued.

In PCI the underestimation of SCF over Southern Hemisphere oceans in January is more pronounced than in ECHAM4, although TCC is higher and LWP is the same as in ECHAM4. The higher TCC is caused by an increase in cloud ice (cf. Fig. 2). Water clouds have been shifted into higher altitudes leaving LWP unchanged. In PCI N_l is lower than in ECHAM4 in all altitudes over the Southern Hemisphere oceans. Since clouds with the same liquid water content are less reflective for fewer but larger droplets, SCF is lower in PCI.

Chen and Roeckner (1996) conclude that the large shortwave cloud forcing (SCF) in ECHAM4 in the tropics results most likely from the neglect of cloud inhomogeneities in the unresolved scales and not from the overestimation of LWP. According to investigations of Davis et al. (1990) and Calahan et al. (1994) the albedo of an optically thick but nonhomogeneous cloud is lower than that of a homogeneous cloud with the same liquid water content, even in the case of an unbroken marine stratocumulus cloud deck. The resulting shortwave albedo bias as observed from stratocumulus clouds in FIRE can be as large as 15%. In PCI the zonal mean LWP is reduced in the tropics up to 15% in July as compared to ECHAM4 and, thus, SCF is reduced by a similar percentage, which makes the effect of cloud inhomogeneities redundant. With respect to the LWP retrieval from Greenwald et al. (1993) one could argue that LWP in the subtropics in both simulations is not overestimated but SCF is too high, which must, therefore, be due to cloud inhomogeneities. On the other hand LWP in the subtropics is too high compared to the retrieval of Weng and Grody (1994), and, consequently SCF should be overpredicted. Thus more observations of LWP as well as more knowledge about three-dimensional cloud inhomogeneities are needed before one reasonably can account for these effects in GCMs.

The relative importance of the aerosol distribution on precipitation formation in warm clouds and the new ice phase scheme for the overall differences between ECHAM4 and PCI are hard to judge because of nonlinearities between the different processes. For example, the higher evaporation rate used in PCI was necessary to simulate correct cloud forcings. This, on the other hand, has an impact on the relative humidity and cloud development in lower altitudes. Nevertheless the relative importance of the aerosol distribution scheme and the new ice phase scheme might be summarized as follows: the aerosol scheme affects the distribution of LWP and low cloud amount in the absence of mixed-phase processes. The new ice phase scheme changes the distribution of ice clouds and high cloud amount. Additionally it determines the mixed-phase processes and, thus, the lifetime of water clouds due to freezing or riming.

Acknowledgements. We thank T. Greenwald and F. Grody for providing the SSM/I cloud water data. We also thank A. Chlond, L. Levkov, J. Feichter and the anonymous reviewers for useful comments.

References

Albrecht BA (1989) Aerosols, cloud microphysics, and fractional cloudiness. Science 245:1227–1230

Arakawa A (1975) Modelling clouds and cloud processes for use in climate models. GARP Publication Series 16. ICSU/WMO:183–197

Beheng KD (1994) A parametrization of warm cloud microphysical conversion processes. Atmos Res 33:193–206

Berry EX, Reinhardt RL (1973) Modeling of condensation and collection within clouds. DRI Phys Sci Pub 16, University of Nevada

Bigg EK (1953) The supercooling of water. Proc Phys Soc 66:688–694

Boer GJ, McFarlane NA, Laprise R, Henderson JD, Blanchet JP (1984) The Canadian Climate Centre spectral atmospheric general circulation model. Atmosphere-Ocean 22:397–429

Boucher O, Lohmann U (1995) The sulfate-CCN-cloud albedo effect. A sensitivity study with two general circulation models. Tellus 47B:281–300

Boucher O, Le Treut H, Baker MB (1995) Precipitation and radiation modelling in a GCM: introduction of cloud microphysical processes. J Geophys Res 100:16395–16414

Brinkop S, Roeckner E (1995) Sensitivity of a general circulation model to parametrizations of cloud-turbulence interactions in the atmospheric boundary layer. Tellus 47A:197–220

Calahan RF, Ridgway W, Wiscombe WJ, Bell TL, Snider JB (1994) The albedo of fractal stratocumulus clouds. J Atmos Sci 51:2434–2455

Cess RD, Potter GL, Blanchet JP, Boer GJ, Del Genio AD, Déqué M, Dymnikov V, Galin V, Gates WL, Ghan SJ, Kiehl JT, Lacis AA, Le Treut H, Li ZX, Liang XZ, McAvaney BJ, Meleshko VP, Mitchell JFB, Morcrette JJ, Randall DA, Rikus L, Roeckner E, Royer JF, Schlese U, Sheinin DA, Slingo A, Sokolov AP, Taylor KE, Washington MW, Wetherald RT, Yanai I, Zhang MH (1990) Intercomparison and interpretation of climate feedback processes in 19 atmospheric general circulation models. J Geophys Res 95:16601–16615

Chen C, Cotton WR (1987) The physics of the marine stratocumulus-capped mixed layer. J Atmos Sci 44:2951–2977

Chen CT, Roeckner E (1996) Validation of the Earth radiation budget as simulated by the Max Planck Institute for Meteorology general circulation model ECHAM4 using satellite observations of the Earth Radiation Budget Experiment (ERBE). J Geophys Res 101:4269–4287

Claussen M, Lohmann U, Roeckner E, Schulzweida U (1994) A global data set of land-surface parameters. Report 135, Max-Planck-Institut für Meteorologie, Germany

Collins WD, Conant WC, Ramanathan V (1994) Earth radiation budget, clouds and climate sensitivity. In: Calver JG (ed) The chemistry of the atmosphere: its impact on global change. Oxford University Press, Oxford, UK, pp 207–215

Cotton WR, Tripoli GJ, Rauber RM, Mulvihill EA (1986) Numerical simulation of the effects of varying ice crystal nucleation rates and aggregation processes on orographic snowfall. J Climate Appl Meteorol 25:1658–1680

Davis A, Gabriel P, Lovejoy S, Schertzer D, Austin GL (1990) Discrete angle radiative transfer: 3. Numerical results and meterological applications. J Geophys Res 95:11729–11742

Del Genio AD, Yao MS, Kovari W, Lo KKW (1996) A prognostic cloud water parametrization for global climate models. J Climate 9:270–304

Eppel DP, Kapitza H, Claussen M, Jacob D, Koch W, Levkov L, Mengelkamp HT, Werrmann N (1995) The non-hydrostatic mesoscale model GESIMA. Part II: parametrizations and applications. Beitr Phys Atmos 68:15–41

Feichter J, Kjellström E, Rodhe H, Dentener F, Lelieveld J, Roelofs GJ (1996) Simulation of the tropospheric sulfur cycle in a global climate model. Atmos Environ (in press)

Fouquart Y, Bonnel B (1980) Computations of solar heating of the Earth's atmosphere: a new parameterization. Beitr Phys Atmos 53:35–62

Fouquart Y, Isaka H (1992) Sulfur emission, CCN, clouds and climate: a review. Ann Geophys 10:462–471

Fowler LD, Randall DA, Rutledge SA (1996) Liquid and ice cloud microphysics in the CSU general circulation model. Part I: model description and simulated microphysical processes. J Climate 9:489–529

Gates WL (1992) AMIP: the atmospheric model intercomparison project. Bull Am Meteorol Soc 73:1962–1970

Geleyn JF (1981) Some diagnostics of the cloud radiation interaction on ECMWF forecasting model. In: Workshop on radiation and cloud-radiation interaction in numerical modelling. 15–17 Oct. 1980 ECMWF, Reading, UK, pp 135–162

Ghan SJ, Easter RC (1992) Computationally efficient approximations to stratiform cloud microphysics parametrization. Mon Weather Rev 120:1572–1582

Greenwald TJ, Stephens GL, Vonder Haar TH, Jackson DL (1993) A physical retrieval of cloud liquid water over the global oceans using Special Sensor Microwave/Imager (SSM/I) observations. J Geophys Res 98:18471–18488

Gunn KLS, Marshall JS (1958) The distribution with size of aggregate snowflakes. J Meteor 15:452–461

Hahn CJ, Warren SG, London J (1994) Climatological data for clouds over the globe from surface observations, 1982–1991: the total cloud edition ORNL/CDIAC-72 NDP-026A Oak Ridge National Laboratory Oak Ridge, Tennessee, USA

Hegg DA, Hobbs PV, Ferek RJ, Waggoner AP (1995) Measurements of some aerosol properties relevant to radiative forcing on the east coast of the United States. J Appl Meteorol 34:2306–2315

IPCC, Climate Change (1992) The supplementary report to the IPCC scientific assessment. In: Houghton JT, Callander BA, Varney SK (eds), Cambridge University Press, Cambridge, UK

Johnson DW (1993) Parametrisation of the cloud topped boundary layer. Aircraft measurements. In: ECMWF Workshop Proc 'Parametrization of the cloud topped boundary layer', ECMWF, Reading, UK, pp 77–117

Kessler E (1969) On the distribution and continuity of water substance in atmospheric circulations, Meteorol Monogr 32, Am Meteorol Soc

Kiehl JT, Hack JJ, Briegleb BP (1994) The simulated Earth radiation budget of the National Center for Atmospheric Research community climate model CCM2 and comparisons with the Earth Radiation Budget Experiment (ERBE). J Geophys Res 99:20815–20827

King MD, Radke LF, Hobbs PV (1993) Optical properties of marine stratocumulus clouds modified by ships. J Geophys Res 98:2729–2739

Lee JL, Liou KN, Ou SC (1992) A three-dimensional large-scale cloud model: testing the role of radiative heating and ice phase processes. Tellus 44A:197–216

Le Treut H, Li ZX (1988) Using Meteosat data to validate a prognostic cloud generation scheme. Atmos Res 21:273–292

Levkov L, Rockel B, Kapitza H, Raschke E (1992) 3D mesoscale numerical studies of cirrus and stratus clouds by their time and space evolution. Beitr Phys Atmos 65:35–58

Lin YL, Farley RD, Orville HD (1983) Bulk parametrization of the snow field in a cloud model. J Clim Appl Meteorol 22:1065–1092

Lohmann U, Roeckner E, Collins WD, Heymsfield AJ, McFarquhar GM, Barnett TP (1995) The role of water vapor and convection during the Central Equatorial Pacific Experiment (CEPEX) from observations and model simulations. J Geophys Res 100:26229–26245

Lord SJ, Willoughby HE, Piotrowicz JM (1984) Role of parametrized ice-phase microphysics in an axialsymmetric, nonhydrostatic tropical cyclone model. J Atmos Sci 41:2836–2848

Malm WC, Sisler JF, Huffman D, Eldred RA, Cahill TA (1994) Spatial and seasonal trends in particle concentration and optical extinction in the United States. J Geophys Res 99:1347–1370

Manabe S, Smagorinsky J, Strickler RF (1965) Simulated climatology of a general circulation model with a hydrological cycle. Mon Weather Rev 93:769–798

Mason BJ (1971) The physics of clouds. Clarendon Press, Oxford

Matveev LT (1984) Cloud dynamics. Atm Sci Library, Reidel, Dordrecht

McFarlane NA, Boer GJ, Blanchet JP, Lazare M (1992) The Canadian Climate Centre second-generation general circulation model and its equilibrium climate. J Climate:1013–1044

McFarquhar GM, Heymsfield AJ (1996) Microphysical characteristics of three anvils sampled during the Central Equatorial Pacific Experiment (CLEPEX). J Atmos (in press)

Mölders N, Laube M, Kramm G (1994) A scheme for parametrizing ice and water clouds in regional models. Proc of EUROTRAC Symp 1994, Borrell et al. (eds), SPB Academic Publishing, The Hague, The Netherlands, pp 839–844

Morcrette JJ (1991) Radiation and cloud radiative properties in the European Centre for Medium Range Weather Forecasts forecasting system. J Geophys Res 96:9121–9132

Murakami M (1990) Numerical modeling of dynamical and microphysical evolution of an isolated convective cloud – The 19 July 1981 CCOPE cloud. J Meteorol Soc Japan 68:107–128

Nordeng TE (1994) Extended versions of the convective parameterization scheme at ECMWF and their impact on the mean and transient activity of the model in the tropics. Tech Memo 206, 41 pp, Euro Cent for Medium Range Weather Forecasts, Reading, England

Novakov T, Penner JE (1993) Large contribution of organic aerosols to cloud-condensation-nuclei concentrations. Nature 365:823–826

Ose T (1993) An examination of the effects of explicit cloud water in the UCLA GCM. J Meteorol Soc Japan 71:93–109

Potter BE (1991) Improvements to a commonly used cloud microphysical bulk parametrization. J Appl Meteorol 30:1040–1042

Pruppacher HR, Klett JD (1978) Microphysics of clouds and precipitation. Reidel, Dordrecht

Radke LF, Coagley JA Jr, MD King (1989) Direct and remote sensing observations of the effects of ships on clouds. Science 246:1146–1149

Ramanathan V, Cess RD, Harrison EF, Minnis P, Barkstrom BR, Ahmad E, Hartmann D (1989) Cloud-radiative forcing and climate: results from the Earth Radiation Budget Experiment. Science 243:57–63

Rangno AL, Hobbs PV (1994) Ice particle concentrations and precipitation development in small continental cumuliform clouds. Q J R Meteorol Soc 120:573–601

Rasch PJ, Williamson DL (1990) Computational aspects of moisture transport in global models of the atmosphere. Q J R Meteorol Soc 116:1071–1090

Rockel B, Raschke E, Weyres B (1991) A parametrization of broad-band radiative transfer properties of water, ice and mixed clouds. Beitr Phys Atmos 64:1–12

Roeckner E (1995) Parameterization of cloud radiative properties in the ECHAM4 model. In: WCRP Workshop "Cloud microphysics parametrizations in global atmospheric circulation models", 23–25 May 1995, WCRP-90, Kananaskis, Canada, pp 105–116

Roeckner E, Schlese U (1985) January simulation of clouds with a prognostic cloud cover scheme. In: ECMWF Workshop "Cloud cover parametrization in numerical models", 26–28 Nov. 1984, ECMWF, Reading, UK, pp 87–108

Roeckner E, Arpe K, Bengtsson L, Brinkop S, Dümenil L, Esch M, Kirk E, Lunkeit F, Ponater M, Rockel B, Sausen R, Schlese U, Schubert S, Windelband M (1992) Simulation of the present-day climate with the ECHAM model: impact of model physics and resolution. Report 93, Max-Planck-Institut für Meteorologie, Germany

Rossow WB, Schiffer RA (1991) ISCCP cloud data products. Bull Am Meteorol Soc 72:2–20

Rossow WB, Walker AW, Garder LC (1993) Comparison of ISCCP and other cloud amounts. J Climate 6:2394–2418

Rutledge SA, Hobbs PV (1983) The mesoscale and microscale structure and organization of clouds and precipitation in midlatitude cyclones. VII: a model for the "Seeder Feeder" process in warm-frontal bands. J Atmos Sci 40:1185–1206

Slingo JM (1987) The development and verification of a cloud prediction scheme for the ECMWF model. Q J R Meteorol Soc 113:899–927

Smagorinsky J (1960) On the dynamical prediction of large-scale condensation by numerical methods. In: Physics of Precipitation, Geophys Mono 5, Am Geophys Union:71–78

Smith RNB (1990) A scheme for predicting layer clouds and their water content in a general circulation model. Q J R Meteorol Soc 116:435–460

Sundqvist H (1978) A parametrization scheme for non-convective condensation including prediction of cloud water content. Q J R Meteorol Soc 104:677–690

Sundqvist H, Berge E, Kristjansson JE (1989) Condensation and cloud parametrization studies with a mesoscale numerical weather prediction model. Mon Weather Rev 117:1641–1657

Tiedtke M (1989) A comprehensive mass flux scheme for cumulus parametrization in large-scale models. Mon Weather Rev 117:1779–1800

Warneck P (1988) Chemistry of the natural atmosphere. Int Geophys Series 41, Academic Press, San Diego, USA

Weng F, Grody NC (1994) Retrieval of cloud liquid water using the special sensor microwave imager (SSM/I). J Geophys Res 99:25535–25551

Xu KM, Krueger SK (1991) Evaluation of cloudiness parametrizations using a cumulus ensemble model. Mon Weather Rev 119:342–367

Young KC (1993) Microphysical processes in clouds. Oxford University Press, New York